Dissolution, bioactivity and osteogenic properties of composites based on polymer and silicate or borosilicate bioactive glass

A. Houaoui, I. Lyyra, R. Agniel, E. Pauthe, J. Massera, Michel Boissière

HAL Id: hal-02498385
https://hal.science/hal-02498385

Submitted on 20 Jul 2022

Dissolution, bioactivity and osteogenic properties of composites based on polymer and silicate or borosilicate bioactive glass

A. Houaoui[1], I. Lyyra[2], R. Agniel[1], E. Pauthe[1], J. Massera[2], M. Boissière[1]

1. ERRMECe, Equipe de Recherche sur les Relations Matrice Extracellulaire-Cellules (EA1391), Institut des matériaux I-MAT (FD4122), Université de Cergy-Pontoise, Maison Internationale de la Recherche (MIR), rue Descartes, 95001 Neuville sur Oise Cedex, France

2. Laboratory of Biomaterials and Tissue Engineering, Faculty of Medicine and Health Technology and BioMediTech Institute, Tampere University, Korkeakoulunkatu 3, 33720 Tampere, Finland
Corresponding author: michel.boissiere@u-cergy.fr

Abstract: Bioactive glass (BAG)/Poly (Lactic Acid) (PLA) composites have great potential for bone tissue engineering. The interest in these materials is to obtain a scaffold with tailorable properties bringing together the advantages of the composites' constituents such as the biodegradability, bioactivity and osteoinduction. The materials studied are PLA/13-93 and PLA/13-93B20 (20% of SiO_2 is replaced with B_2O_3 in the 13-93 composition). To characterize them, they were dissolved in TRIS buffer and Simulated Body Fluid (SBF) in vitro. Over the 10 weeks of immersion in TRIS, the ion release from the composites was constant. Following immersion in SBF for 2 weeks, the hydroxyapatite (HA) layer was found to precipitate at the composites surface. By adding Boron, both these reactions were accelerated, as the borosilicate glass dissolves faster than pure silicate glass alone. Polymer degradation was studied and showed that during immersion, the pure PLA rods maintained their molecular weight whereby the composites decreased with time, but despite this the mechanical properties remained stable for at least 10 weeks. Their ability to induce osteogenic differentiation of myoblastic cells was also demonstrated with cell experiments showing that C2C12 cells were able to proliferate and spread on the composites. The Myosin Heavy Chain and Osteopontin were tracked by immunostaining the cells and showed a suppression of the myosin signal and the presence of osteopontin, when seeded onto the composites. This proves osteoinduction occurred. In studying the mineralization of the cells, it was found that BAG presence conditions the synthesizing of mineral matter in the cells. The results show that these composites have a potential for bone tissue engineering.

Keywords: Bioactive Glass, Composite material, Osteogenic differentiation

Introduction

Bioresorbable polymers have been used widely in the past decades as pins, plates and screws in orthopaedic, cranial and oral surgery[1–4]. The bioresorption of the implants enables leaving the fixation in place until it degrades in the body, releasing non-toxic dissolution by-products which are then metabolised[5]. However, the bioresorbable polymers developed thus far clinically, are found to degrade at slow rate and lack osteoconductive properties[1,6]. Bioceramics are a class of materials grouping all traditional nearly inert ceramics such as, Al_2O_3 and ZrO_2, and include calcium phosphate ceramics and silicate bioactive glass (BAG). These demonstrate properties extending from bioresorbable to bioactive class A. Clinically, β-TCP (bioresorbable) and synthetic hydroxyapatite (HA) (bioactive) are the more widely used traditionally[1,7,8], but their slow dissolution rate is a limiting factor[9,10]. Indeed, concerns have been addressed pertaining to the limited resorption of those ceramics, in-vivo, when used in cements[11]. BAG is a sub-category of ceramics showing not only osteoconduction, as in synthetic HA, but also osteoinduction[12]. These glasses are commercialized mainly for hard tissue reconstruction, but they also show significant ability to bond to soft tissue[13]. However, shaping the glass into its final shape is, as for all ceramics, challenging.

The quest for bioresorbable implants which are osteoconductive for use in the treatment of traumas in the skeletal system is still ongoing and presents significant challenges still. To overcome some of the drawbacks of single materials, composites have been developed. Here, the focus will be on polymer/BAG composites, as previous studies have demonstrated that fast release of ions from BAG compensated for the decrease in pH due to the rapid degradation of Poly (Lactic acid-co Glycolic Acid) (PLGA)[14]. By adding BAG to (Poly (D,L-Lactic Acid) (P(D,L)LA) or Poly (Lactide-co-Caprolactone) (PLCL)) the mechanical properties increases as well as precipitation of an HA layer at the composite scaffold surface[15,16]. These studies used the solvent-casting method. Vergnol et al. developed composites based on P(L,DL)A/45S5

BAG. In this study, glass particles (3.5µm average diameter) were mixed with polymer dissolved in acetone. The pellets obtained were then injected into molds at 145°C and 150 bars of pressure. The presence of the BAG not only increased the rate of degradation of the polymer, but also significantly promoted new bone formation in this animal study[17]. However, there was a large loss in polymer molecular weight reported over the course of the sample processing. The decrease in molecular weight could not only be assigned to the processing temperature but also to the presence of the BAG particles[18]. The mechanical properties of the scaffold were also found to decrease drastically over the short immersion time in vitro. The loss in mechanical properties seemed to be correlated with the loss in the mineral phase, which is assumed to be fast given the rapid dissolution rate of the small BAG particles. Another study by Niemelä et al. presents self-reinforced composites based on P(L,DL)A/13-93 BAG, made by twin-screw extrusion at temperatures varying between 190 and 195°C. In this study, the particle size was between 50 and 125µm. It is noteworthy, that not only 13-93 is slower dissolving than 45S5 (at similar particle size), but also the larger particle size will further slowdown the dissolution rate of the inorganic phase[19,20]. Degradation of the self-reinforced composites was evaluated in PBS and the results supported the effect of glass dissolution on the polymer degradation rate[19]. The 13-93 particles contained in the self-reinforced composite create a porosity which induces a degradation of the polymer due to acidic dissolution products coming from the environment. The use of 13-93 in the composites appeared to retain higher polymer molecular weights than when using faster dissolving glasses such as 45S5 or S53P4. To overcome the slow dissolution rate of 13-93, boron can replace the silica in the structure, yielding a borosilicate glass. The resulting borosilicate and borate glasses, based on the 13-93 composition, show faster in-vitro dissolution and also faster conversion into HA[21,22]. While high boron content was associated with a decrease in the cell proliferation rate, it was also found to stimulate osteogenic commitment and upregulate endothelial markers[22]. In-vivo and in-

vitro studies have shown the promising nature of borosilicate glasses[19,23]. The use of borate and borosilicate glasses as a secondary phase in a polymeric matrix has not yet been widely studied. Taino et al. produced PLCL (Poly(L-lactide-co-ε-caprolactone)/borosilicate glass composites, with varying content of 125-250 µm glass particles using the solvent-casting method. These scaffolds were then foamed by supercritical CO_2. Degradation of the polymer was linked to the dissolution of the glass[15].

Marquardt et al. studied the processing of fibrin / borate glass composites obtained by mixing fibrin with glass microfibers $0.5 - 10\,\mu m$ diameter, or with rods of $50 - 200\,\mu m$ diameter which were placed on a fibrin scaffold prior to polymerization. The materials obtained were able to support directed axon growth[24].

However, the effect of boron substitution for silica, in the glass composition, on the composite physico-chemical properties and cell / material interaction has not yet been studied. Added to this, based on previously reported results, the use of glass 13-93 and its boron-containing counterpart might be suitable in maintaining polymer integrity and composite mechanical properties in-vitro while supporting osteogenesis. Therefore, we have developed PLA/BAG composites using 13-93 as control and 13-93B20 with 20% SiO_2 replaced by B_2O_3. To investigate the in vitro dissolution behavior of our composites, they were immersed in TRIS buffer solution. Ion release from the glass and change in the polymer molecular weight were quantified. The mechanical properties of the composites were studied during the immersion. The bioactivity, assumed to be related to the precipitation of a HA layer at the surface of the material when immersed in aqueous solution, was assessed in Simulated Body Fluid (SBF), the procedure usually used for testing BAG[25]. Preliminary cell experiments were done to assess cell activity and ability of these two BAG to promote osteogenesis by culturing C2C12 myoblastic cells at the surface of composite discs. Cell proliferation and morphology were studied as well as presence of myosin and/or osteopontin which were tracked by

immunostaining. C2C12 cells capacity to synthesize their mineral matrix was analyzed with Alizarin Red S staining. The aim of this study was to assess if these cells were able to commit to an osteoblastic lineage in presence of the BAG.

Experimental

1. **Material preparation and characterization**

    1.1. **Bioactive glass (BAG) preparation**

    BAG 13-93 and 13-93B20 were prepared from analytical grade K_2CO_3 (Alfa Aesar, Haverhill, USA), (Na_2CO_3, $NH_4H_2PO_4$, $(CaHPO_4)(2(H_2O))$, $CaCO_3$, MgO, H_3BO_3 (Sigma Aldrich, Saint-Louis, MS, USA) and Belgian quartz sand. The 100-gram batches of 13-93 and 13-93B20 were melted for 3 hours in a platinum crucible at 1425°C and 1275°C, respectively. The molten glasses were cast, annealed, crushed and finally sieved into 125-250µm particles. The glasses were dried at 125°C for 2 hours before use. The nominal oxide compositions of the glasses are given in Table 1.

Table 1: Nominal glass composition (mol%)

Glass	mol%						
	Na_2O	K_2O	MgO	CaO	P_2O_5	SiO_2	B_2O_3
13-93	6.0	7.9	7.7	22.1	1.7	54.6	--
13-93B20	6.0	7.9	7.7	22.1	1.7	43.7	10.9

    1.2. **Sample Fabrication**

    Medical grade Poly(Lactic Acid) (PLA) with a (L/DL) ratio of 70/30, with an inherent viscosity of 4.0dl/g was obtained from Evonik Nutrition & Care GmbH (Essen, Germany). PLA, PLA/13-93 and PLA/13-93B20 rods were produced by melt-extrusion using a co-rotating twin-screw extruder (Mini ZE 20*11.5 D, Neste Oy, Porvoo, Finland) under nitrogen

atmosphere (Figure 1). The feed rates for the PLA and the BAG were fixed to 140g.h^{-1} and 60g.h^{-1} respectively to obtain approximately 70wt. % of polymer and 30wt. % of glass in the composite. The processing temperatures and pressures are presented in Table 2. The polymer took about 5 minutes to produce in the extruder including melting and producing the final product. The production time is less when the extruder is filled in advance.

Table 2: Materials processing parameters

	Temperature (°C)			Pressure (psi)
	Cylinder	Adapter	Die	
PLA rods	200	230	230	200
PLA/13-93	190	200	220	150
PLA/13-93B20	185	220	215	200

A 4 mm nozzle was used and the rods were pulled using a caterpillar. The speed of the caterpillar was adjusted to obtain 3 mm diameter rods.
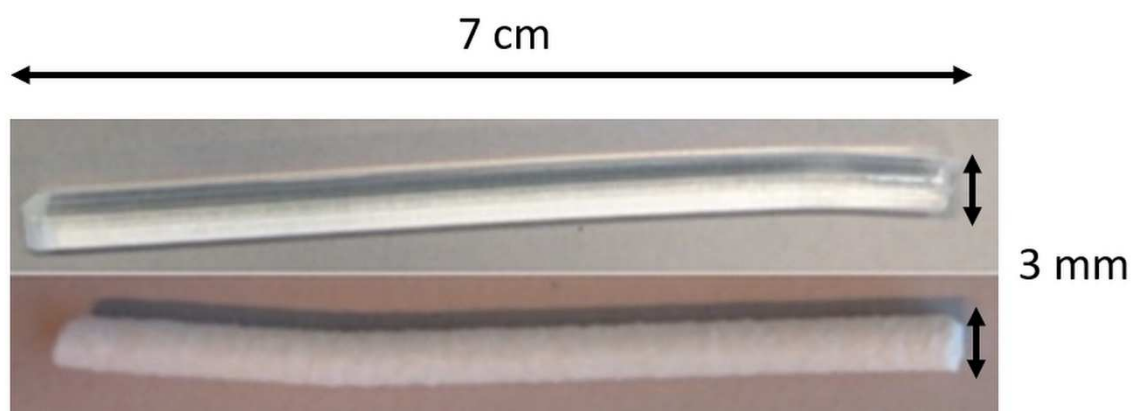

Figure 1: PLA rod (up) and composite rod (down) obtained after extrusion

The rods of each composition (PLA as a control; PLA/13-93; PLA/13-93 B20) were analyzed by Thermogravimetric Analysis (NETZSCH, Leading Thermal Analysis, STA449F1) to measure their glass content. All tests were performed in an Alumina (Al_2O_3) crucible and in a N_2 atmosphere. 10 mg of sample were heated from 25 °C to 1100 °C at a rate of 10 °C/min.

This measurement was repeated on 5 samples for each composite and the average glass content with standard deviation was calculated.

2. Behavior of the PLA/BAG composites

2.1. Physico-chemical properties of the composites

2.1.1 Immersion in TRIS

Tris(hydroxymethyl)aminomethane (TRIS) solution (50mM) was prepared by mixing ultra-pure TRIS (MP Biomedicals) and TRIS-HCl (Sigma Aldrich) in ultra-pure water and the pH was adjusted to 7.4 at 37°C. The rods were cut into lengths of 7cm ($\simeq$650 mg) which were immersed in 12mL of TRIS solution for up to 10 weeks at 37°C in a shaking incubator (HT Infors Multitron) at an orbital speed of 100rpm. To avoid saturation of the solution with the ions released from the composite, the TRIS buffer was refreshed each week.

At set times after immersion, the concentration of elements released from the composites was studied by diluting 5mL of the immersion solution in 45mL of ultra-pure water for ion analysis. ICP-OES (Agilent technologies 5110) was employed to quantify P (λ = 253.561 nm), Ca (λ = 422.673 nm), Mg (λ = 279.553 nm), Si (λ = 250.690 nm), B (λ = 249.678nm), K (λ = 766.491 nm) and Na (λ = 589.592 nm) concentrations in the solution after sample immersion. Measurements were made on four separate samples at each set time for each composite and the results presented as mean ± standard deviation (SD). The rods were then rinsed with acetone and dried.

2.1.2 Rod cross section analysis

After immersion in TRIS, the samples were embedded in resin and then polished to observe their cross section using Scanning Electron Microscopy (SEM - GEMINISEM 300 from Zeiss).

2.1.3 Molecular weight of the polymer

Molecular weights of PLA after the samples processing and at various immersion times were determined by Gel Permeation Chromatography (GPC) (Merck Hitachi Lachrom 7000 series) consisting of a pump, a refractive index detector and two Waters Styragel columns (HR5E and HR1). Tetrahydrofuran (THF) was used as eluent at a flow rate of 1 mL/min at 35°C. For each material, an amount of $\simeq$7,5mg of polymer (cross-section of the rod) was weighed and immersed in 5mL of THF until complete dissolution. The solution was then filtered and analyzed. Molecular weights were calibrated using polystyrene standards. The measurements were conducted in four separate samples at each time points for each composition and the results are presented as mean ± SD.

2.1.4 Mechanical properties of the composites

The mechanical properties of the composite rods post-processing and after immersion (wet) were tested on the Instron 4411 (Instron Ltd., High Wycombe, UK) using a 3-point bending and shear test at room temperature. At least four parallel samples of each composite type were tested. For the bending test, the properties were studied with a crosshead speed of 5 mm.min^{-1} and a bending span of 42 mm. For the shear test[26], the crosshead speed was 3 mm.min^{-1}. The measurements were conducted in the four samples at each set point for each composite and the results are presented as mean ± SD.

2.2 Composites bioactivity

2.2.1 Immersion in Simulated Body Fluid (SBF)

SBF was prepared following the methodology[27] from the standard ISO/FDIS 23317 as described by Kokubo et al. The samples were cut to obtain rods of 7cm ($\simeq$650 mg) which were immersed in 12mL SBF solution for up to 2 weeks at 37°C in a shaking incubator (HT Infors Multitron) with at a speed of 100rpm. During the experiment, the solution was not refreshed so that calcium phosphate could be measured. The ion concentration in the solution according to

immersion time was measured as previously described. Measurements were made on four separate samples at each set time for each composite and the results presented as mean ± SD.

2.2.2 Rod surface analysis

The reactive layer at the rod surface after immersion in SBF was observed by SEM (GEMINISEM 300 from Zeiss) and its composition was analyzed by Energy-Dispersive X-ray spectroscopy (EDX Quantax from BRUKER). The Infrared (IR) absorption spectra of the composites immersed in SBF were also recorded using a Bruker Alpha FTIR in Attenuated Total Reflectance (ATR) mode to see the effect of the dissolution on their structural properties. The measurements were performed on dry samples. All IR spectra were recorded within the range 399–4000 cm^{-1} with a resolution of 2 cm^{-1} and 32 accumulation scans.

2.3 Cell analysis

2.3.1 Disk preparation

PLA, PLA/13-93 and PLA/13-93B20 disks were obtained by compression molding (Nike Hydraulics ZB110, Eskilstuna, Sweden) of a piece of the rods for the cellular tests. The rods were compressed under 10-20 MPa pressure at 140 °C for 1 min, then the mold was cooled down with compressed air and 14mm disks were cut from the plates obtained. These disks were then sterilized by gamma irradiation (25 kGy) at BBF sterilisations service GmbH (Germany). All experiments were performed in 24-well plates and the disks were washed with PBS prior to use.

2.3.2 Cell culture

Myoblastic C2C12 cells were cultured in DMEM Glutamax supplemented with 10 % Fetal Bovine Serum (FBS) and 1 % penicillin/streptomycin, in an humidified atmosphere of 5 % CO_2 at 37 °C.

2.3.3 Cell proliferation and morphology

To compare the behavior of C2C12 cells on the different samples, cell proliferation was studied using CyQUANT Cell Proliferation Assay kit (Invitrogen, Life Technologies). Around 7700 cells/disk were seeded on the 14mm disks in 24-well plate and the medium was changed every 2 days. Cleaned and sterilized microscope glass slides were used as controls. After 1, 2, 4 and 7 days of culture, the cells were lysed with 400 µL 0.1 % Triton-X100 (Sigma–Aldrich) buffer and conserved at -80 °C. After one freeze–thaw-cycle, three 20 µl aliquots of each lysate were pipetted on to a black 96-well plate (Corning) and mixed with 180 µl working solution (CyQUANT GR dye and cell lysis buffer). The fluorescence was then measured at 520nm with a Spectrofluorimeter Xenius XM (SAFAS).

The morphology of the cells on the different samples was observed after 48 h of culture. The same number of cells was seeded on the disks and after 48 h, the cells were fixed with 3 % (w/v) para-formaldehyde solution dissolved in PBS (Sigma Aldrich) for 15 min, then permeabilized with 0.1 % (v/v) Triton X-100 (Sigma Aldrich) for 10 min. Non-specific binding sites were blocked by incubating the disks in PBS containing 1 % Bovine Serum Albumin (BSA) for 1 h. The cytoskeleton and nuclei of the cells were stained respectively with 1:500 FITC-labelled phalloidin (Sigma Aldrich P5282) and 1:1000 4',6-Diamidino-2-phenylindole dihydrochloride (DAPI, Sigma Aldrich D9542) in PBS-BSA 0.5 % for 1 h. Each incubation with antibodies was performed in the dark in a humid atmosphere. Samples were then washed in PBS-BSA 0.5 %, mounted in Prolongold (Invitrogen), and observed under a LSM710 confocal microscope (Carl Zeiss).

2.3.4 Cell differentiation

The expression of a late myoblastic marker (myosin heavy chain) and an early osteoblastic marker (osteopontin) were studied using specific antibodies. Around 600 C2C12 cells were seeded on the disks and cultured for 14 days. Cleaned and sterilized microscope glass slides

were used as controls. Cells were then labelled with mouse anti-myosin heavy chain (MHC, 1:1000, Millipore 05716), and rabbit anti-osteopontin (1:500, Millipore AB10910) diluted in PBS containing 0.5 % BSA. Primary antibodies are revealed using Alexa Fluor 488 or Alexa Fluor 568-conjugated goat anti-mouse or anti-rabbit antibodies both 1:400 in PBS-BSA 0.5 % (Invitrogen) as secondary antibodies. Samples were observed using a LSM710 confocal microscope (Carl Zeiss).

Mineralization was also assessed at 10 days and 14 days using Alizarin Red S stain (the calcium minerals stain red). The staining from a previously described protocol was adjusted[28] in that cells were fixed with paraformaldehyde for 15min at room temperature and stained with 2 % Alizarin red S (pH 4.1–4.3; Sigma–Aldrich) for 20 min at room temperature. The excess color was washed away with three consecutive water washes after which the samples were observed under an optical microscope.

2.3.5 **Statistical analysis**

Data were analyzed using GraphPad Prism Software. Statistical significance between groups is assessed by one-way analysis of variance (ANOVA). Experimental results are expressed as means ± standard deviation. Statistical significance is taken for values of $p < 0.05$.

Results and discussion

The aim of this study was to develop a polymer-BAG composite able to release ions beneficial for bone regeneration while maintaining, post-processing, the mechanical properties and the molecular weight of the polymer. As it has been reported that it is difficult to produce a polymer-bioglass ® (i.e. 45S5) composite, we decided to incorporate BAG 13-93 into a PLA matrix. As reported by Brink et al. the dissolution rate of the glass 13-93 is much slower than the typical BAG used clinically (*i.e.* 45S5 (Bioglass®) and S53P4 (BonAlive®)[20]). To

control glass dissolution, a second glass composite was tested [23], whereby 20% of the SiO_2 in the 13-93 composition was replaced with B_2O_3.

1. Characterization of the composites after processing

Table 3 presents the glass loading in each composite, with the mechanical properties of the composites and the molecular weight of the polymer included in each composite.

Table 3: Measured glass loading, mechanical properties and average molecular weight of the processed PLA and PLA/BAG composites (for wet samples, the mechanicals properties were measured after 10min of immersion in TRIS).

Materials	Composites glass loading (wt%)	Young modulus (GPa)		Shear stress (MPa)		PLA Mw before extrusion (kDa)	PLA Mw after extrusion (kDa)
		Dry samples	Wet samples	Dry samples	Wet samples		
Bulk PLA	--	--	--	--	--	526 ± 7	--
PLA rods	--	3.5 ± 0.1	3.6 ±0.2	46.6 ± 0.8	50.1 ± 1.4	--	305 ±14
PLA/13-93 rods	38 ± 2	3.6 ± 0.3	3.3 ± 0.3	34.0 ± 2.0	32.3 ± 1.4	--	248 ± 5
PLA/13-93B20 rods	35 ± 4	3.6 ± 0.7	3.1 ± 0.4	32.1 ± 1.5	32.1 ± 1.1	--	251 ± 15

The targeted glass loading was 30 wt%. Thermogravimetric analysis was conducted (Figure S1) to assess the true glass loading in the polymer matrix post-processing as well as the homogeneity of the processed rods. Glass loading was 38±2 wt% and 35±4 wt% for the PLA/13-93 and PLA/13-93B20, respectively, demonstrating good control over the process used to produce the composites.

Before extrusion, the molecular weight of the PLA granules was measured to be ~530 kDa. As expected, after extrusion, the molecular weight of the pure PLA decreased about 40 %, while the PLA loaded with BAG decreased by ~50% regardless of the glass composition. The decrease of the molecular weight recorded is not as high as that reported in the literature. For example, Vergnol et al. show a decrease in molecular weight of ~90% when producing PLA-BAG composite processed by injection molding[17]. Moreover, the PLA/S53P4

composites were tested, but, during the processing the viscosity of the polymer drastically and rapidly decreased and the materials obtained were amber-like as reported by Vergnol et al. for the PLA/45S5. The reason for this rapid change in viscosity and subsequent thermal degradation of the PLA is not yet well understood. However, this phenomenon appears when processing PLA with fast reacting BAG and does not occur that readily with more stable glasses. Therefore, a hypothesis for the thermal degradation of PLA upon extrusion of composites using 45S5 and/or S53P4 may be due to the high intrinsic water content in the glass structure or the glass degradation/dissolution when in the polymer melts. The combination of PLA and the proposed BAG 13-93 processed by twin-screw reduces loss of molecular weight during melt processing.

The mechanical properties of the PLA and its composites were measured in 3-point bending and shear. Both composites have an almost stable flexural modulus in wet and dry conditions but show a decrease in shear stress in both conditions, when compared to the polymer alone. The changes in the mechanical properties are only a function of the glass loading but not due to the nature of the glass. The decrease in the shear strength was not unexpected, since polymer glass composites are known to become weaker, and tend to become more brittle, as can be seen by an increase in their elastic modulus. Here, the decrease in the flexural modulus indicates an increase in the ductility. Such behavior, was already reported in self-reinforced polymer/BAG filaments[26]. The loss in mechanical properties is probably due to the absence of chemical bonds between the glass and the polymer, leading to a loss of cohesivity.

2. Behavior of the composites in solution

2.1 Dissolution in TRIS

The co-degradation in TRIS of the polymer and glass was assessed by GPC and ICP-OES measurements and compared to that of the dissolution of the pure PLA rods. Figure 2

13

presents the concentration in Si A), Na B), K C), B D), Mg E), Ca F) and P G) post immersion in TRIS for various times. As the immersion solution was refreshed every week the results are presented cumulatively and normalized to the sample mass. As expected, the PLA alone does not exhibit any change in ion concentration. Upon immersion of the composites, the concentration in solution of the different elements increases, indicating that the glass particles are being hydrated and dissolve through the polymer. As expected, the addition of boron to the glass structures leads to faster initial ion release (up to ~10 days). However, at longer immersion times all curves seem to plateau for solutions containing the PLA/13-93B20 composites whereas the dissolution of the glass in the PLA/13-93 composite remains almost linear. It should be noted that; especially at longer immersion times, the standard deviation was higher in the case of the polymer containing the glass 13-93B20 than 13-93.

It is a known fact that upon immersion of a silicate glass in aqueous solution, initially ion exchange occurs followed by condensation and re-polymerization of a silica-rich layer[12]. If this layer is not uniformly formed at the surface of all glass particles, variations in ion release can be expected. All ion concentrations were normalized to the element contained in the starting rod to show clearly the extent of ion release.
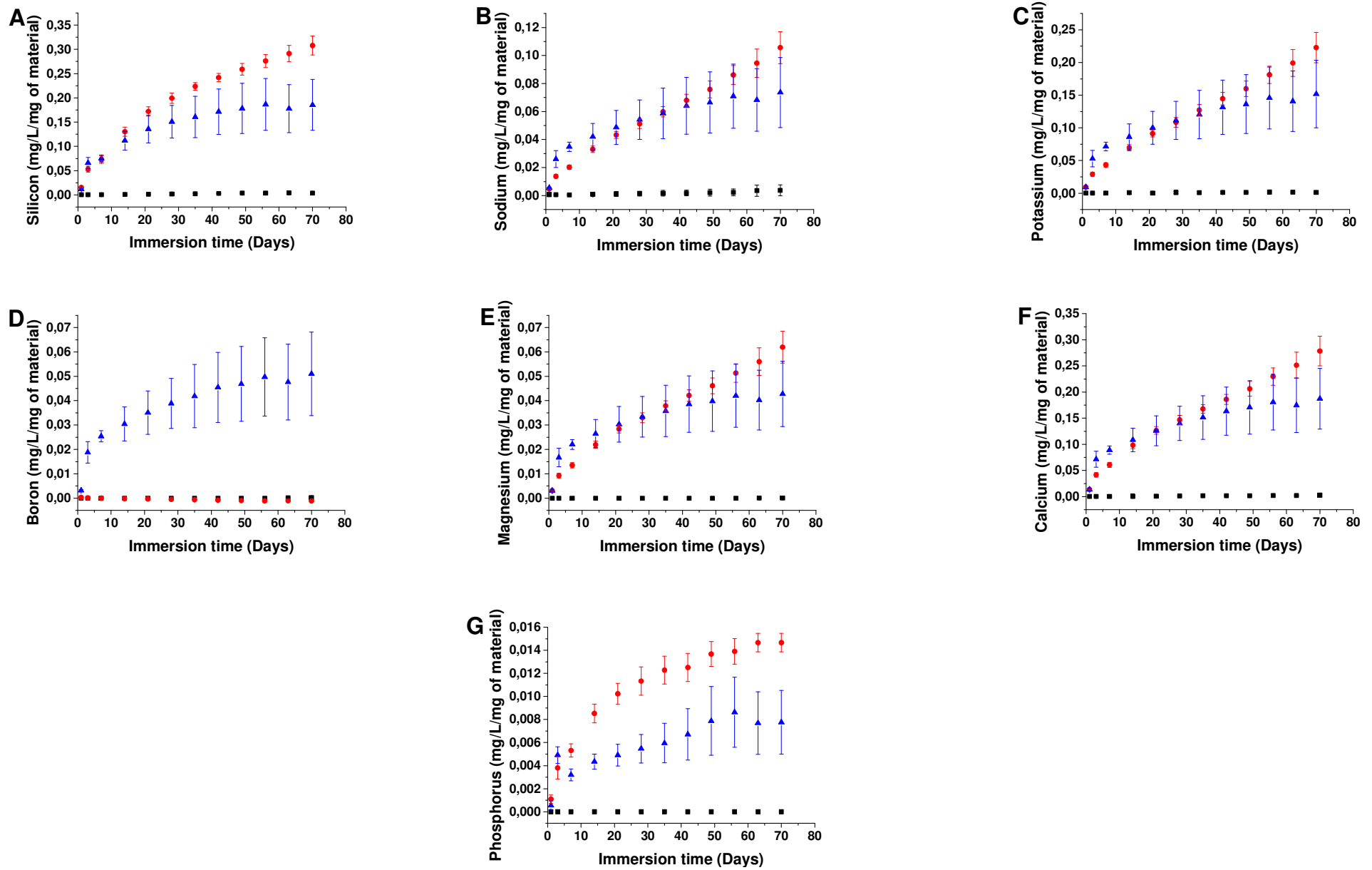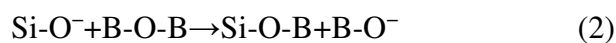
Figure 2: Element concentrations of A) Si, B) Na, C) K, D) B, E) Mg, F) Ca and G) P in the dissolution products of PLA (■), PLA/13-93 (●) and PLA/13-93B20 (▲) immersed in TRIS according to time.

Figure 3A) presents the percentage of ion released from glass 13-93 in TRIS solution. It is clear that glass dissolution is limited, whereby at 70 days less than 5% of each element is released into the solution. While the Si and P release seems to level-off at immersion times >20 days, all other constituents, *i.e.* Na, Ca, Mg and K seemed to be leached-out in an almost linear manner up to 70 days. Figure 3B) presents the release of ion from the glass 13-93B20, in % of initial mass of the elements. As seen in the case of the composites containing the glass 13-93, all ions are found to leach out into the solution. However, the difference in the dissolution profile of ions from the composites containing the glass 13-93B20 compared to ion release from composites containing the glass 13-93, is of interest.

1. While in Figure 3A) the Ca, K, Mg and Na dissolve, from the glass 13-93, at similar rate, a slower release of Ca was measured during dissolution of composites containing the glass 13-93B20 (Figure 3B). Furthermore, Ca release follows a similar dissolution profile to B as shown in Figure 3B).

2. The initial release rate for all ions is faster for composites containing the glass 13-93B20. However, at extended immersion time (>15 days) a decrease in the release rate of all ions can be seen; whereas when immersing composites containing the glass 13-93 (Figure 3A) only Si and P release rate slows down at extended immersion time, while all other ions show a linear release.

3. The final ion release content in the solution (at 70 days) is slightly lower in the case of the composite containing the glass 13-93B20 than in that containing the glass 13-93.

From the literature many interactions between the B_2O_3 and SiO_2 in the glass were reported to happen. Some are reported below [29–32]:

$$2Si\text{-}O^- + B\text{-}O\text{-}B \rightarrow Si\text{-}O\text{-}Si + 2B\text{-}O^- \qquad (1)$$

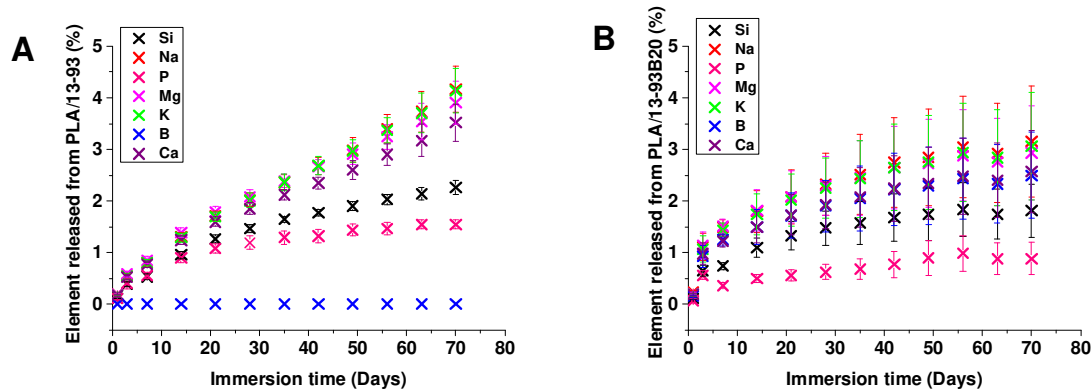$$Si\text{-}O^- + B\text{-}O\text{-}B \rightarrow Si\text{-}O\text{-}B + B\text{-}O^- \qquad (2)$$

Figure 3: Release of ions from the A) PLA/13-93 and B) the PLA/13-93B20, immersed in TRIS according to time.

However, those reactions were not sufficient to explain the physical, thermal and structural changes associated with the substitution of the SiO_2 with B_2O_3. In depth structural analysis showed preferential interaction between CaO and B_2O_3 as follow [33]:

$$BO_3 + CaO \leftrightarrow BO_4 \qquad (3)$$

More recently, Yu et al. reported the medium-range structural organization of phosphorus bearing borosilicate glasses and the consequence of B/Si substitution [34]. Their findings support the increase in the polymerization of the silica network with increasing substitution ratio. Furthermore, they demonstrated a higher affinity of the phosphorus to bond with B rather than with Si. Therefore, while in typical silicate glass the majority of the phosphorus is present as Q^0 (zero bridging oxygen atom per PO_4 unit), an increase in Q^1 units, bridging one oxygen atom per PO_4 unit, was evidenced. Overall, the structural modification occurring in the glass network when substituting Si for B is in agreement with the dissolution behavior observed in Figure 3A) and B), i.e. boron and calcium are released at the same rate (Figure 3B) as typically seen in a congruent dissolution. Thus, it appears that the calcium preferentially interacts with the boron sub-network (congruent dissolution) rather than with the silicate sub-network (non-congruent dissolution). The lower, overall release of the ions (at long immersion time) is most likely related to the increase in the degree of polymerization of the silica network as shown in equations 1 and 2, where the number of non-bridging oxygen is

17

expected to decrease with increasing the boron content. However, such structural analysis does not fit the dissolution behavior reported in the literature, which tend to demonstrate that the addition of B_2O_3 at the expense of SiO_2 should increase the glass dissolution rate[35–38]. It is therefore possible to assume that either the increase in Si-O-Si bridges is associated with a disproportionation of the silicate structure, whereby, $2Q^2 \leftrightarrow Q^1 + Q^3$, and/or Si-O-B bridges form between the borate and silicate units. Both assumptions would be consistent with the increase in the initial dissolution rate of the glass in the composite containing the glass 13-93B20 and a progressive decrease in the ion release rate due to remnants of a more stable silicate. As seen in Figure 3A) and B), this leads to a higher ion concentration in the solution containing the borosilicate glass at a short immersion time, and saturation occurring at an earlier time than in the case of traditional silicate BAG such as 13-93. Finally, the increased linkages between the phosphorus structural unit and the more stable BO_4 units proposed by Yu et al.[34] is confirmed by the lower phosphorus release profile in the case of the glass 13-93B20 than in 13-93.

Figure 4 shows the cross sections of the composites before and after 10 weeks of immersion in TRIS. Before immersion, the BAG granules are fixed and appear to be maintained by the PLA matrix. After 10 weeks in TRIS, they are seen to be detached from the polymer, regardless of the glass composition, as expected post surface dissolution of the glass particles.

At the same time, the change in the polymer molecular weight was assessed according to time and is presented in Figure 5. Although the extrusion process affected the PLA molecular weight (Mw), it does not seem to be impacted by the interaction with the medium after immersion for up to 10 weeks. However, slow but linear molecular weight decrease is apparent during immersion of the composite. The composite containing the BAG 13-93, showed the fastest PLA degradation with a loss of ~45% of its molecular weight post-extrusion at 10 weeks at a rate of 1710 ± 96 Da / day (R^2=0.99).
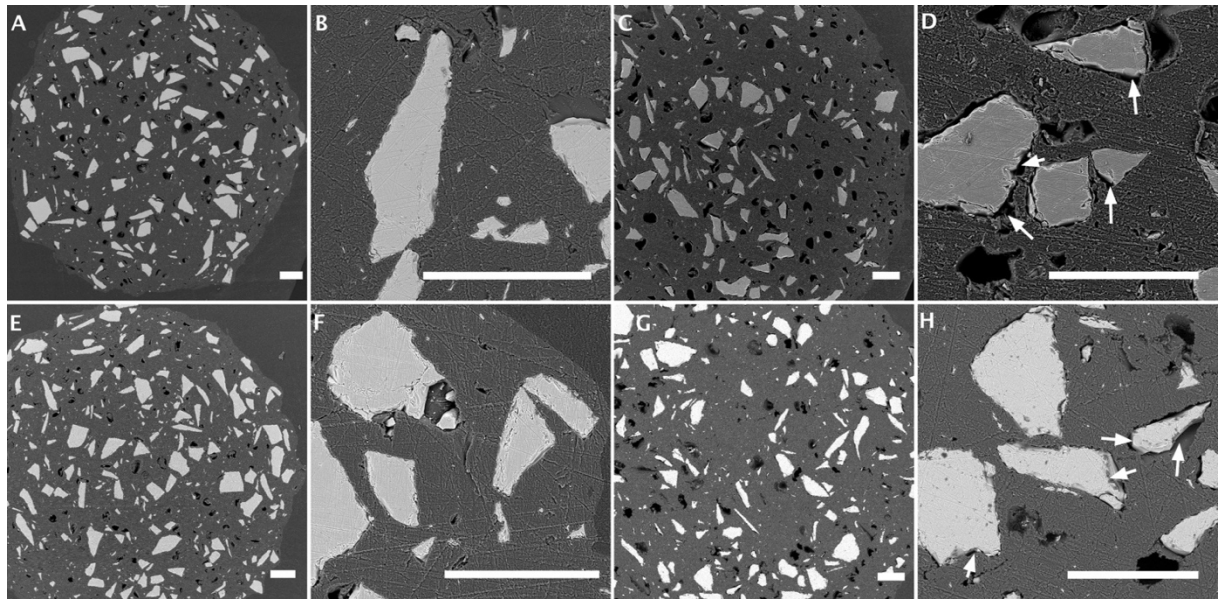
Figure 4: Observations of the cross section of the composites by SEM. A) and B) show the PLA/13-93 before immersion, C) and D) show the PLA/13-93 after 10 weeks of immersion in TRIS. E) and F) present the PLA/13-93B20 before immersion and G) and H) show the PLA/13-93B20 after 10 weeks of immersion in TRIS. Scale bar 200µm
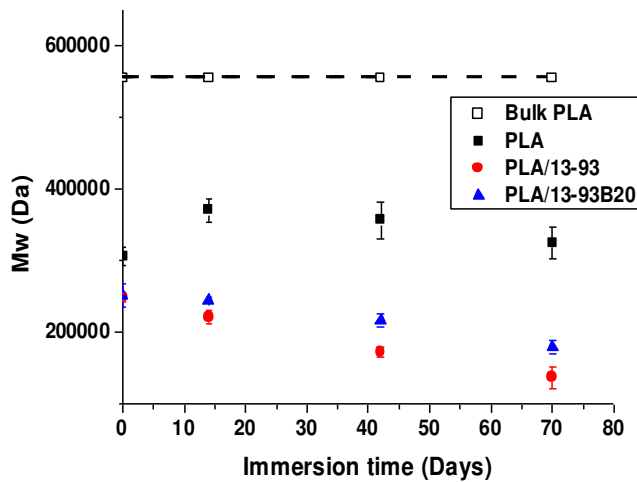

Figure 5: Molecular Weight (Mw) of PLA before extrusion (□) PLA (■), PLA/13-93 (●) and PLA/13-93B20 (▲) rods immersed in TRIS according to time.

The composite containing the BAG 13-93B20 showed a slower decrease, of ~29 % of its original molecular weight after 10 weeks of immersion at a rate of 1133 ± 82 Da / day (R^2=0.98). In both cases, the degradation of the polymer is due to the interaction between glass dissolution by-products and PLA, most likely by alkaline hydrolysis of ester bonds at the glass/PLA interface[39]. Such behavior was, however, not reported by Maquet et al. with the

dissolution of bioglass®-filled polylactic foams but occurred during dissolution of PLA/BAG composite in vivo[16,17]. Added to this, the difference in PLA degradation can be related to the more sustained ion release in the case of the composite containing the glass 13-93 as seen in Figure 3.
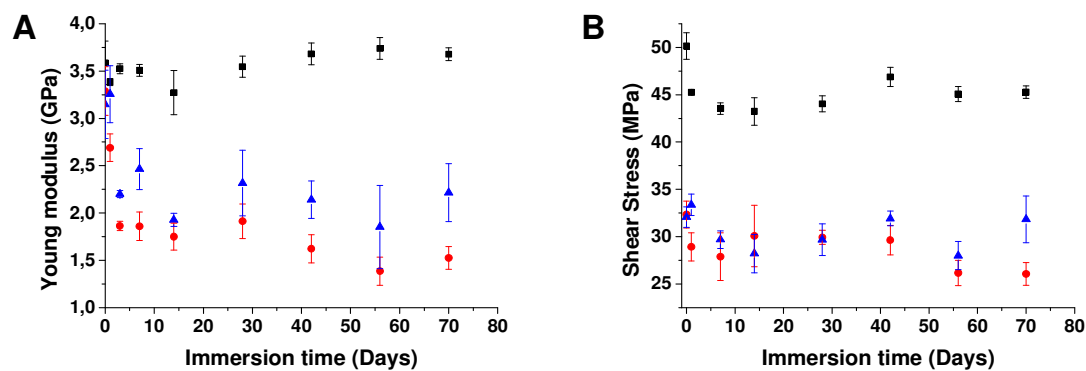

Figure 6: A) Young modulus reported from the bending test and B) Shear stress of wet PLA (■), PLA/13-93 (●) and PLA/13-93B20 (▲) rods according to immersion time in TRIS.

The mechanical properties (Young modulus and Shear stress) were measured on wet samples as a function of immersion time (Figure 6). While no significant changes in shear stress, within the accuracy of the measurement, were recorded, a net fall in the Young modulus can be seen after immersion for up to three days. As all the measurements were corrected to the swelling of the sample, such a drop can be attributed to the diffusion of water within the composite structure, most likely due to pores being formed during the processing. After the initial drop, the Young modulus does not seem to be, drastically, impacted by either the glass or the polymer dissolution/degradation.

Upon immersion of composites in TRIS buffer solution, a decrease in the average molecular weight was measured. However, in this study and in agreement with data reported by Vergnol et al, the decrease of the PLA molecular weight alone could not be correlated to changes in the mechanical properties[17]. Yet, in Vergnol et al., a decrease in mechanical properties was recorded upon immersion of the BAG/PLA composite. The loss in mechanical strength is directly related to the composite mass loss with regards to the immersion time.

20

Therefore, the dissolution of mineral phase dictated the change in mechanical properties. In our study, the larger particle size of BAG with slower dissolution rate than in Vergnol et al's work were used[17]. The low dissolution rate of the BAG used in this study implies that the composite keeps its integrity for at least 10 weeks.

The immersion of the composites in TRIS helped to understand the dissolution of both composites in solution. The 13- 93B20 dissolves faster initially than the 13-93 and saturates more quickly to the same level as the 13-93 in the end. This dissolution leads to the decrease of the polymer molecular weight, but the mechanical properties stay almost stable.

2.2 Dissolution in SBF

Samples were also immersed in Simulated Body Fluid (SBF). As postulated by L.L. Hench, the ability of a material to induce the precipitation of an hydroxyapatite layer at its surface is considered to be a sign of bioactivity[12].

Immersion in SBF was conducted over a two weeks period and the solution was not refreshed. ICP-OES was used to quantify the ion concentration in the solution. The difference between the ion concentration in SBF and ion concentration post composite immersion was calculated (Figure 7).

The elements Si, K, Mg and B (for the PLA/13-93B20) show similar trends when immersed in TRIS where the 13-93B20 glass leaches out its ions at a faster rate initially and then stabilizes. However, it is important to point out that i) the dissolution rate starts to slow down at an earlier immersion time in SBF than in TRIS and ii) while limited saturation was noticed, in the case of immersion of the PLA/13-93 in TRIS buffer solution, in SBF, saturation can also be seen for this glass. The Ca concentration seems to increase initially and then decreases with increasing immersion time, whereas the P concentration decreases constantly over dissolution time. Generally, the decrease in Ca and P in SBF is associated with the precipitation of a calcium-

phosphate reactive layer. The decrease in Ca and P is faster and starts at earlier time when the composites containing BAG 13-93B20 are immersed, indicating a faster and more rapid precipitation of the reactive layer in the case of this material. This is most likely due to the faster initial dissolution.
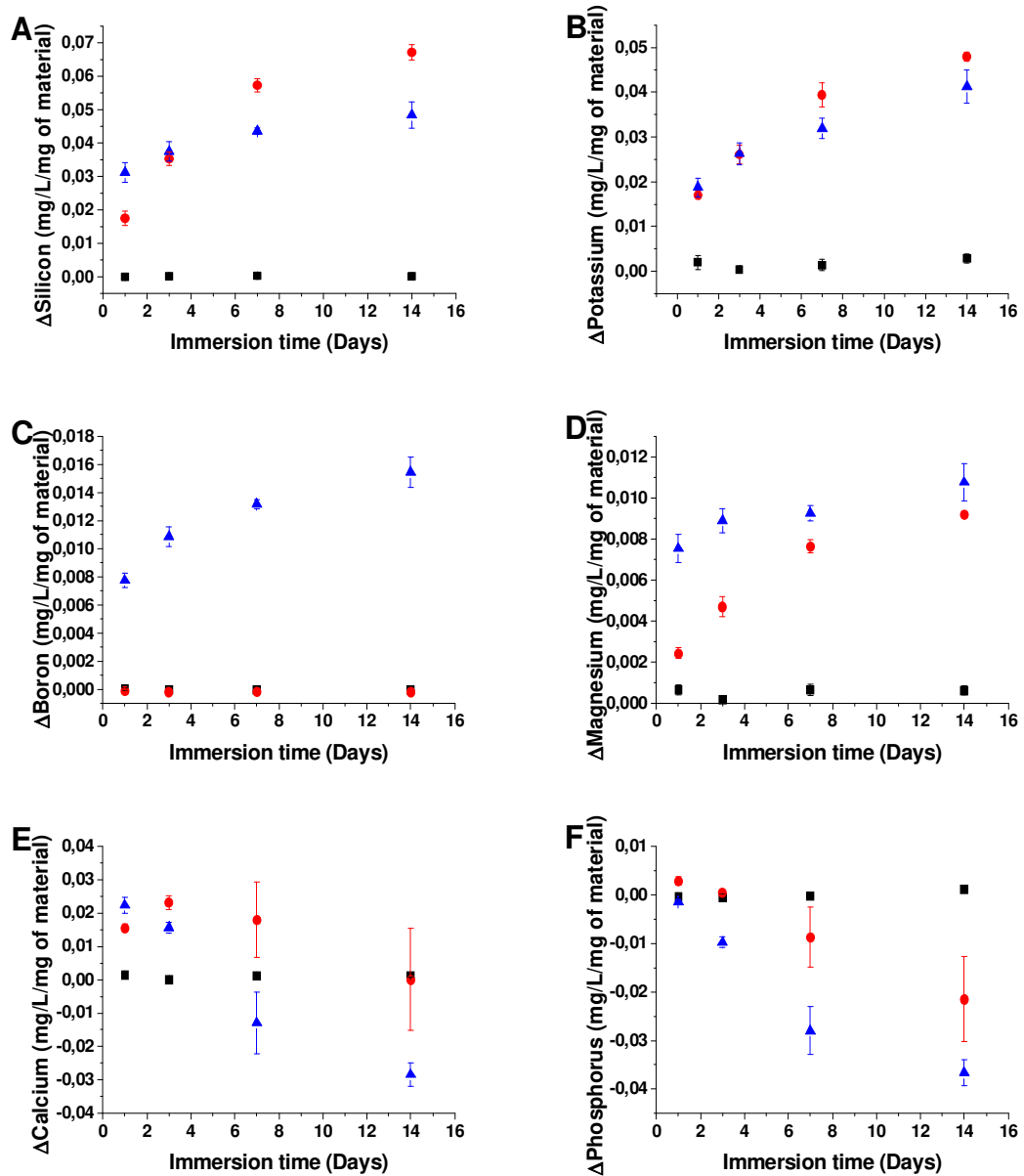

Figure 7: A) Si, B) K, C) B, D) Mg, E) Ca and F) P element concentrations released in SBF from the PLA (■), PLA/13-93 (●) and PLA/13-93B20 (▲) according to immersion time. ΔElement = [Element] in SBF in presence of the sample – [Element] in SBF initial solution.

The precipitation of a reactive layer at the surface of the rods was assessed by SEM/EDX and FTIR. Figure 8) presents the SEM images of the PLA (A and B), PLA/13-93 (C and D) and PLA/13-93B20 (E, F and G) before and after 14 days of immersion in SBF.
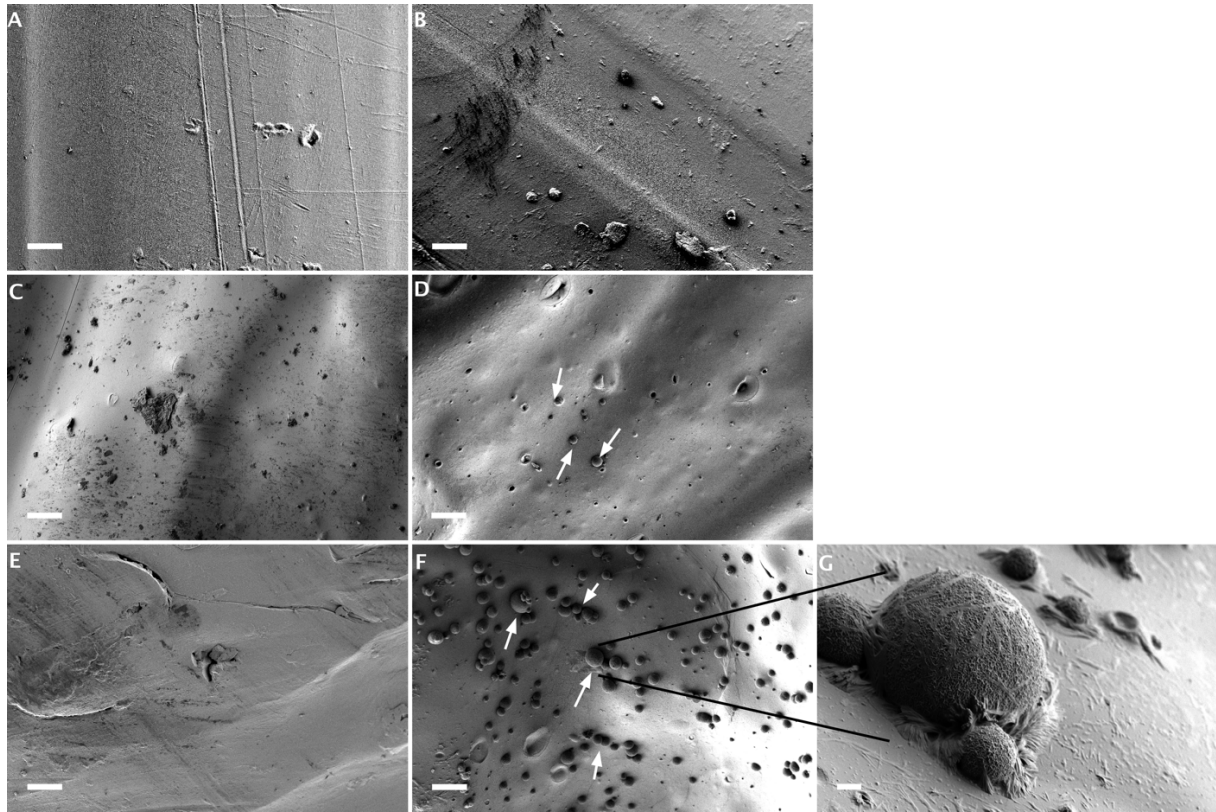

Figure 8: Surface observations and analysis by SEM-EDX and FTIR of the PLA and the composites. A) and B) show the surface of the PLA before and after 2 weeks of immersion in SBF respectively. C) and D) represent the PLA/13-93 before and after 2 weeks of immersion in SBF. E) and F) show the PLA/13-93B20 before and after 2 weeks of immersion in SBF (Scale bar 20µm) and G) represents the nodules found on the PLA/13-93B20 after 2 weeks in SBF (Scale bar 2µm).
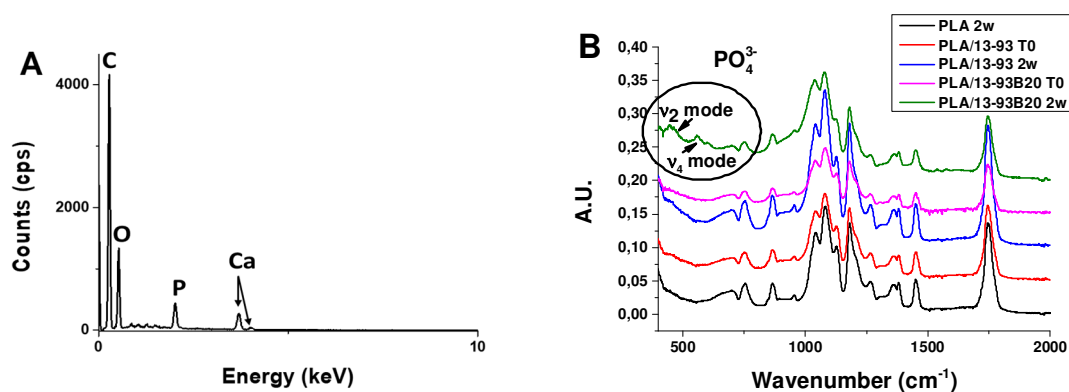

Figure 9: A) EDX analysis of the nodules found on PLA/13-93B20 surface and B) FTIR analysis of the sample surfaces before and after 2 weeks of immersion.

While no significant change in the surface topography can be seen after immersion of the PLA in SBF, some spheres could be seen at the surface of the composites after 14 days. The spheres were small and sparsely dispersed at the surface of the composites containing the glass 13-93 (Figure 8D), while higher density of larger spheres (with a wide size distribution) were covering the composites containing the glass 13-93B20 (Figure 8F). This is in agreement with the faster reactive layer formation hypothesized from the ICP analysis for the boron containing composites.

EDX was performed on the spheres showed on Figure 8G) and an EDX spectra is presented in Figure 9A). The composition of the sphere is mainly Ca and P with a Ca/P ratio of ~1.6. This is a good indication that the calcium phosphate layer precipitating is hydroxyapatite. This was further confirmed by FTIR spectroscopy shown in Figure 9B). While only peaks related to the PLA structure where seen in the pure PLA and PLA/13-93 composite, prior and after immersion in SBF, whereas two peaks in the 400-600 cm^{-1} appeared after PLA/13-93B20 immersion in SBF. These peaks are characteristic of the ν_4 (P – O bending) and ν_2 (O – P – O bending) PO_4^{3-} vibration in apatite structure[40,41]. This effect is partially overcome when working with 13-93B20. The particles are mainly embedded in PLA which slows the release rate due to the PLA diffusion barrier. However, one should keep in mind that despite 13-93B20 promoting more effective HA precipitation than 13-93, a similar reactivity to 45S5 or S53P4 has not yet been reached.

We developed PLA/BAG composites using a process that enables limiting the polymer degradation while maintaining mechanical properties which are of interest in bone tissue engineering. Furthermore, the inorganic filler dissolved when immersed in aqueous solution with kinetics function of the glass composition. The PLA/13-93B20 composite was also found to precipitate a hydroxyapatite layer upon immersion in SBF. Therefore, we decided to do

preliminary cell experiments to assess if these composites have potentially osteogenic properties which are of utmost important in bone reconstruction.

3. C2C12 proliferation and morphology

The C2C12 cell system was chosen owing to its known dependence by adhesion to the substrate rigidity, and to the experimental ease in measuring the cellular response to the Bone Morphogenetic Protein 2 (BMP-2). In addition, this cell line is important and relevant in the progenitor cell system for bone tissue engineering[42].

Firstly, the proliferation of C2C12 cells on PLA and both composites was studied for up to 7 days (Figure 10).
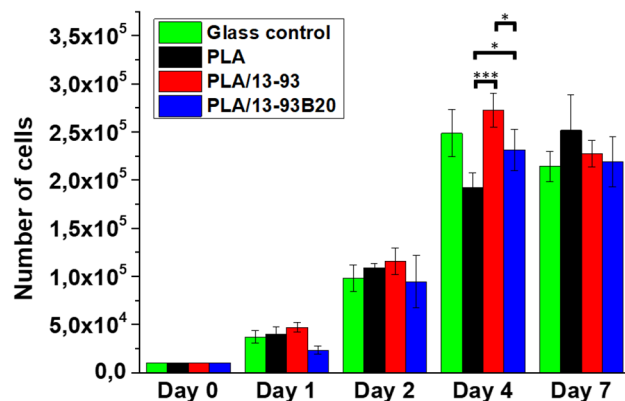

Figure 10: Proliferation of C2C12 cells cultured in DMEM complete medium on glass, PLA, PLA/13-93 and PLA/13-93B20 for 7 days, analyzed with a CyQUANT Cell Proliferation Assay kit, ***p<0.001, *p<0.05.

Glass slides were used as a control. The cells proliferated with the characteristic profile of this cell phenotype on all substrates. At 4 days, the proliferation of C2C12 cells on the composites is significantly higher than on the PLA alone. Fu et al. and Eqtesadi et al.[23,43] have already demonstrated that 13-93 glass alone promotes cell adhesion and proliferation. It is interesting to point out, that at day 4, the cell count is statistically higher at the surface of the PLA/13-93 than on the PLA/13-93B20. This is certainly due to the release of boron from the borosilicate

glass, which is known to decrease cell proliferation while promoting osteogenesis[44]. It can also be seen that the morphology of murine C2C12 myoblasts after 48h of incubation (Figure 11), seem to spread more within the cytoskeleton of the cells with PLA/13-93 and PLA/13-93B20, than with PLA alone.

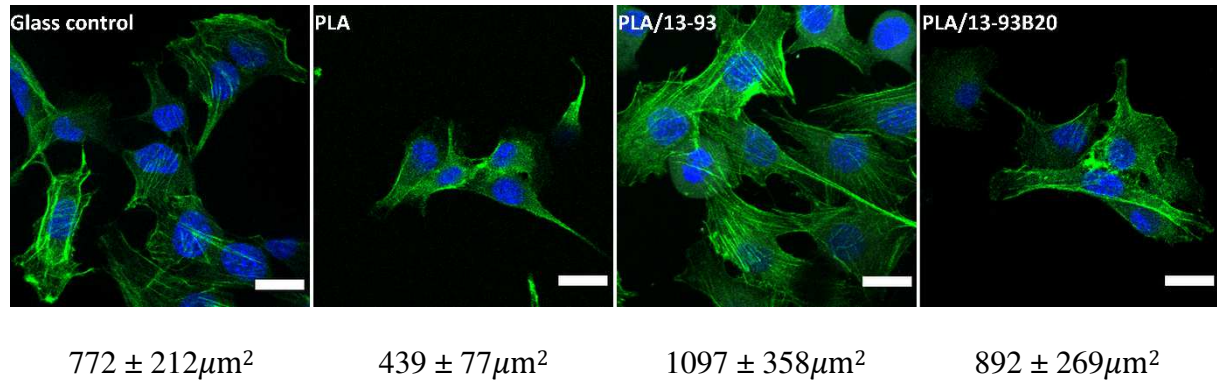| Glass control	PLA	PLA/13-93	PLA/13-93B20
$772 \pm 212 \mu m^2$	$439 \pm 77 \mu m^2$	$1097 \pm 358 \mu m^2$	$892 \pm 269 \mu m^2$

Figure 11: Morphology observations of C2C12 cells in DMEM complete medium analyzed by immunostaining, Nuclei (DAPI - blue) and Actin (Phalloidin - green), after 48h of incubation on glass, PLA, PLA/13-93, PLA/13-93B20 (Scale bar 20µm). Under each image the spreading area of the cells is annotated on each sample after 48h of incubation.

This is confirmed by the measurements of the spreading surface of the cells on each material (Figure 11). The lower ability of the cells to spread on PLA can be correlated to slightly slower proliferation of cells at day 4 (Figure 10), when compared to proliferation on composites. Thereby, both types of BAG do not present cytotoxic effects and when included in the PLA, they promote proliferation and adhesion of C2C12 cells compared to the PLA alone.

4. C2C12 differentiation

In order to study the capacity of C2C12 cells to commit to an osteoblastic lineage in presence of BAG, myosin heavy chain (late marker of myogenic differentiation) and osteopontin (early marker of osteoblastic differentiation) were stained after 14 days of incubation.

In Figure 12, it can be seen that the glass control (Figure 12B and C) and pure PLA (Figure 12F and G) have a high myosin expression but no osteopontin expression. The

differentiation of C2C12 myoblasts into myotubes can be observed. With a BAG load into the PLA, myosin expression is decreased and osteopontin expression becomes visible (Figure 12J, K, N, O). This expression seems higher for the cells seeded on the composite containing 13-93B20 and myosin expression seems completely suppressed. Clearly, the osteopontin, marker of osteoblastic differentiation, is significantly expressed in cells cultured on the composites and this expression seems higher when using the borosilicate glass in PLA. However, the marker needed quantifying to confirm the effect of the boron included in the glass formulation compared to the silicate glass. C2C12 cells are often used to study osteodifferentiation in presence of BMPs[42,45]. Here, their capacity to differentiate into osteoblastic cells is exploited in the presence of BAG showing promising results for osteodifferentiation.

Mineralization was investigated using Alizarin Red Staining after 10 and 14 days of culture. This product stains the mineral calcium. As 10 days appeared to be too short a time to distinguish the mineralization, only images after 14 days of incubation are presented in Figure 13. Figure 13 shows the glass, the PLA, and both composites post staining with Alizarin Red. On the glass control and the PLA without cells (Figure 13A and B), no red staining could be observed with the cells (Figure 13E and F), the staining seen is attributed to the high cell density, and therefore gives an indication of background noise. On both composites without cells, a slight red coloration is observed (Figure 13C and D). As shown in Figure 7, the dissolution of the composites leads to a small amount of HA precipitation. This may well occur within the culture medium and, therefore, the slight red coloration may be due to either, Alizarin being trapped at the glass/PLA interface of stained HA mineral. When the PLA/13-93 and the PLA/13-93B20 are seeded with the cells, strong red staining is evident, showing mineral formation (Figure 13G and H). These results, when compared to the results obtained without cells, suggest that the mineral stained by the Alizarin is not due to the precipitation of HA but

is produced by the cells through their metabolism in presence of the 13-93 or 13-93B20. Therefore, the cells are conditioned by the composites to synthesize their mineral matter.
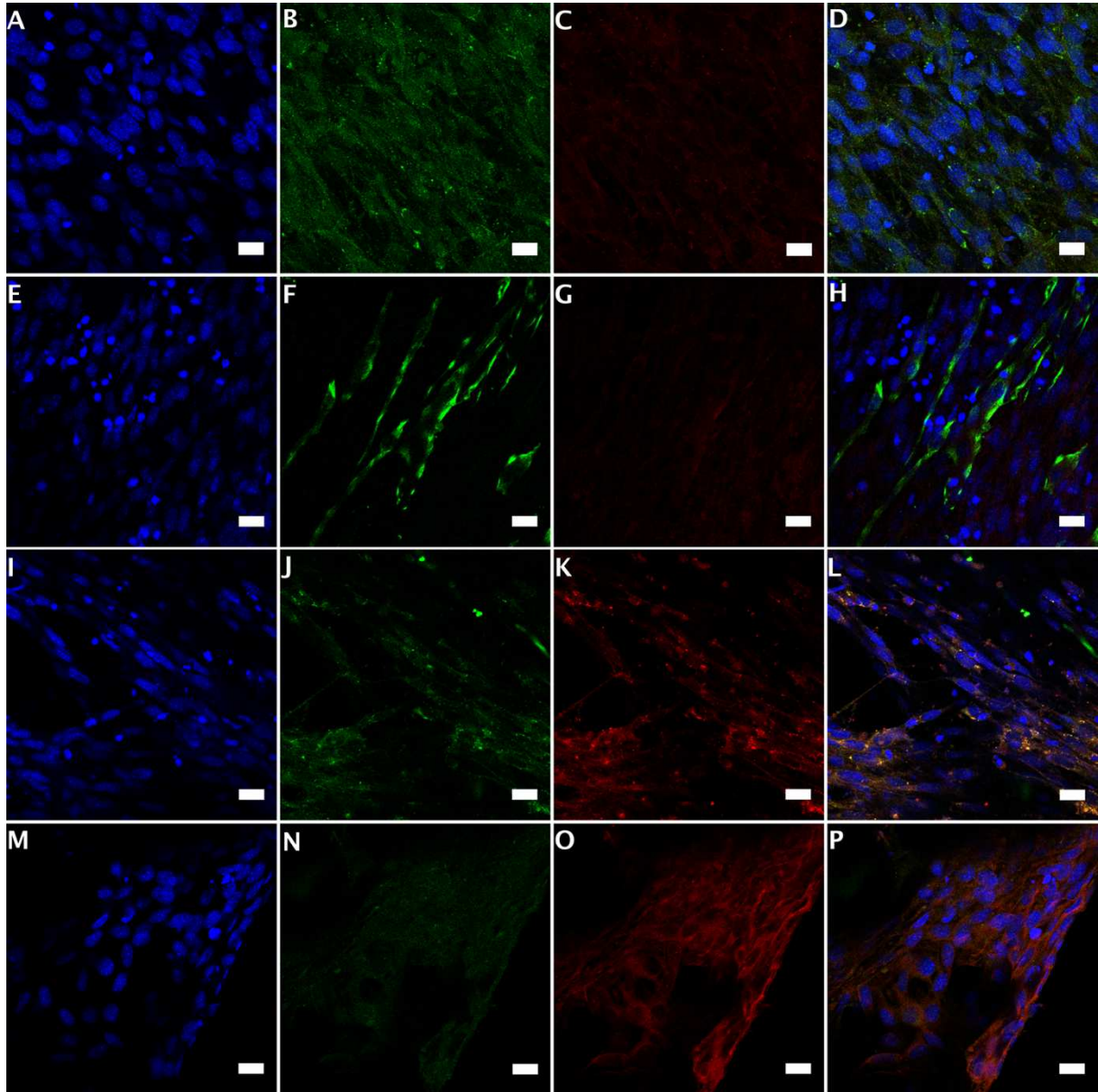

Figure 12: Differentiation of C2C12 cells on glass (A, B, C, D), PLA (E, F, G, H), PLA/13 -93 (I, J, K, L) and PLA/13-93B20 (M, N, O, P) analyzed by Nuclei (DAPI – blue – First column), Myosin (green – Second column), Osteopontin (red – third column) and the merge (fourth column) immunostaining after 14 days of incubation. Scale bar 20µm
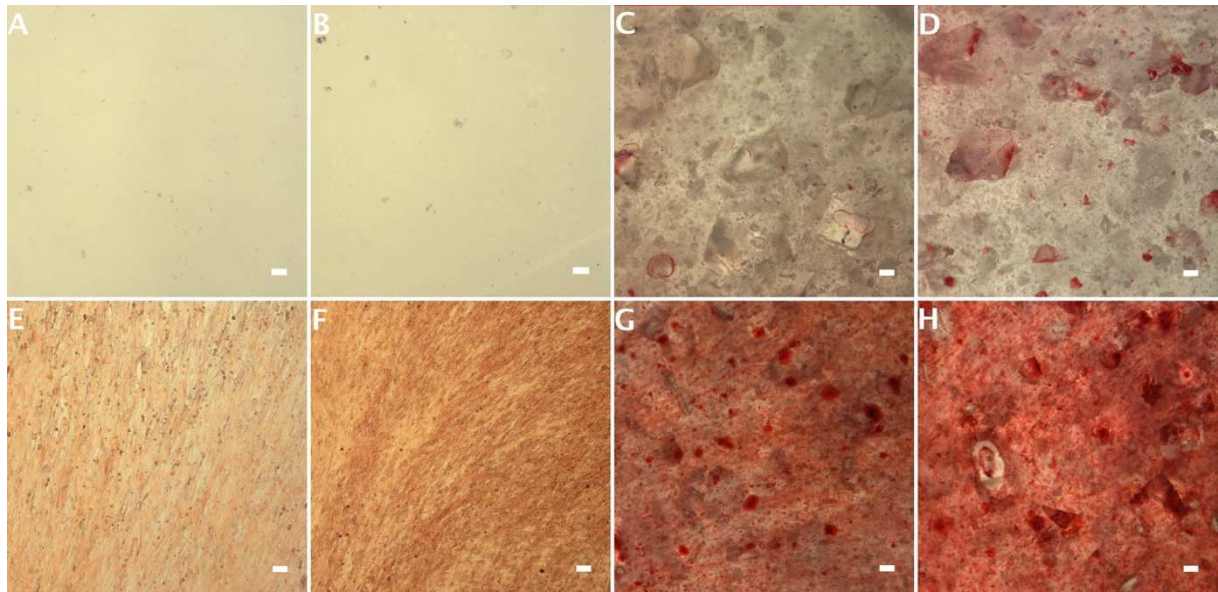
Figure 13: Mineralization of C2C12 cells in DMEM was studied with Alizarin red S staining after 14 days of incubation. The first line shows A) the glass, B) the PLA, C) the PLA/13-93 and D) the PLA/13-93B20 without any cells seeded. The second line represents E) the glass, F) the PLA, G) the PLA/13-93 and H) the PLA/13-93B20 with C2C12 cells seeded for 14 days. Scale bar 200µm

Conclusion

Composites made of PLA and bioactive glasses (silicate 13-93 and borosilicate 13-93B20) were processed by twin-screw extrusion. This process led to composites with content in the organic phase consistent across the length of the filaments and in agreement with the expected loading. The choice of the glass composition, particle size, glass loading, extrusion temperature as well as pressure for extrusion notably reduced the thermal degradation of the PLA, when compared to previous studies performed with similar or other processing techniques. The presence of BAG particles within the PLA matrix leads to a more ductile, but more fragile material as seen in the case of self-reinforced polymer/BAG composites.

The dissolution of the glass is not impaired by the polymeric matrix. As hypothesized, the substitution of part of the SiO_2 in the 13-93 glass composition with B_2O_3 leads to an increase in the initial dissolution rate. In turns, this leads to a higher level of hydroxyapatite precipitation. However, the dissolution of the BAG leads to an increased degradation rate of

the PLA, not affecting the mechanical properties which remained stable for at least 10 weeks. Finally, the dissolution of the composites in SBF support the hypothesis that the developed composites are bioactive, especially in the case of the composite containing the glass 13-93B20.

The osteogenic response of the C2C12 myoblastic cells to both composites – PLA/13-93 and PLA/13-93B20 – was studied. Cells were grown and spread on the composites and the expression of the myosin and the osteopontin measured after 14 days. When cells were cultured on pure PLA, myosin expression was clearly observed while on composites, only osteopontin was expressed. The mineralization experiment showed that the cells in presence of the 13-93 and the 13-93B20 were able to synthesize their mineral matrix.

These composites are promising for bone application. Nevertheless, we feel that more studies are needed to quantify and confirm the effect of the borosilicate at the cellular level.

Conflict of interest

There are no conflicts to declare.

References

[1]   G. Schwach, M. Vert, In vitro and in vivo degradation of lactic acid-based interference screws used in cruciate ligament reconstruction, International Journal of Biological

Macromolecules. 25 (1999) 283–291. doi:10.1016/S0141-8130(99)00043-4.

[2]   L.E. Claes, A.A. Ignatius, K.E. Rehm, C. Scholz, New bioresorbable pin for the reduction of small Gony fkagm.ents: design, mechanical properties and in vitro degradation, 17 (1996) 1621–1626. doi:10.1016/0142-9612(95)00327-4.

[3]   R. Suuronen, Comparison of absorbable self-reinforced poly-L-lactide screws and metallic screws in the fixation of mandibular condyle osteotomies: An experimental study in sheep, Journal of Oral and Maxillofacial Surgery. 49 (1991) 989–995. doi:10.1016/0278-2391(91)90065-T.

[4]   A.R. Santos Jr., Bioresorbable Polymers for Tissue Engineering, in: D. Eberli (Ed.), Tissue Engineering, InTech, 2010. doi:10.5772/8580.

[5]   W.S. Pietrzak, D. Sarver, M. Verstynen, Bioresorbable implants — practical considerations, Bone. 19 (1996) S109–S119. doi:10.1016/S8756-3282(96)00139-1.

[6]   M. Walton, N.J. Cotton, Long-term *in vivo* Degradation of Poly- L -lactide (PLLA) in Bone, Journal of Biomaterials Applications. 21 (2007) 395–411. doi:10.1177/0885328206065125.

[7]   K. Shimazaki, V. Mooney, Comparative study of porous hydroxyapatite and tricalcium phosphate as bone substitute, Journal of Orthopaedic Research. 3 (1985) 301–310. doi:10.1002/jor.1100030306.

[8]   K. Ohura, M. Bohner, P. Hardouin, J. Lemaître, G. Pasquier, B. Flautre, Resorption of, and bone formation from, new ?-tricalcium phosphate-monocalcium phosphate cements: Anin vivo study, Journal of Biomedical Materials Research. 30 (1996) 193–200. doi:10.1002/(SICI)1097-4636(199602)30:2<193::AID-JBM9>3.0.CO;2-M.

[9]   S. Hasegawa, S. Ishii, J. Tamura, T. Furukawa, M. Neo, Y. Matsusue, Y. Shikinami, M. Okuno, T. Nakamura, A 5–7 year in vivo study of high-strength hydroxyapatite/poly(l-lactide) composite rods for the internal fixation of bone fractures, Biomaterials. 27 (2006) 1327–1332. doi:10.1016/j.biomaterials.2005.09.003.

[10]   C.C.P.M. Verheyen, J.R. de Wijn, C.A. van Blitterswijk, K. de Groot, P.M. Rozing, Hydroxylapatite/poly(L-lactide) composites: An animal study on push-out strengths and interface histology, Journal of Biomedical Materials Research. 27 (1993) 433–444. doi:10.1002/jbm.820270404.

[11]   K. Ishikawa, Calcium Phosphate Cement, in: B. Ben-Nissan (Ed.), Advances in Calcium Phosphate Biomaterials, Springer Berlin Heidelberg, Berlin, Heidelberg, 2014: pp. 199–227. doi:10.1007/978-3-642-53980-0_7.

[12]   L.L. Hench, The story of Bioglass®, Journal of Materials Science: Materials in Medicine. 17 (2006) 967–978. doi:10.1007/s10856-006-0432-z.

[13]   R.M. Day, A.R. Boccaccini, S. Shurey, J.A. Roether, A. Forbes, L.L. Hench, S.M. Gabe, Assessment of polyglycolic acid mesh and bioactive glass for soft-tissue engineering scaffolds, Biomaterials. 25 (2004) 5857–5866. doi:10.1016/j.biomaterials.2004.01.043.

[14]   H. Li, J. Chang, pH-compensation effect of bioactive inorganic fillers on the degradation of PLGA, Composites Science and Technology. 65 (2005) 2226–2232. doi:10.1016/j.compscitech.2005.04.051.

[15]   J. Tainio, K. Paakinaho, N. Ahola, M. Hannula, J. Hyttinen, M. Kellomäki, J. Massera, In Vitro Degradation of Borosilicate Bioactive Glass and Poly(l-lactide-co-ε-caprolactone) Composite Scaffolds, Materials. 10 (2017) 1274. doi:10.3390/ma10111274.

[16]   V. Maquet, A.R. Boccaccini, L. Pravata, I. Notingher, R. Jérôme, Preparation, characterization, and *in vitro* degradation of bioresorbable and bioactive composites based on Bioglass®-filled polylactide foams: Porous Polylactide/Bioactive Glass Composites, Journal of Biomedical Materials Research Part A. 66A (2003) 335–346. doi:10.1002/jbm.a.10587.

[17]   G. Vergnol, N. Ginsac, P. Rivory, S. Meille, J.-M. Chenal, S. Balvay, J. Chevalier, D.J. Hartmann, *In vitro* and *in vivo* evaluation of a polylactic acid-bioactive glass composite for

bone fixation devices: POLYLACTIC ACID-BIOACTIVE GLASS COMPOSITE FOR BONE FIXATION DEVICES, Journal of Biomedical Materials Research Part B: Applied Biomaterials. 104 (2016) 180–191. doi:10.1002/jbm.b.33364.

[18] H. Kometani, T. Matsumura, T. Suga, T. Kanai, Quantitative Analysis for Polymer Degradation in the Extrusion Process, International Polymer Processing. 21 (2006) 24–31. doi:10.3139/217.0092.

[19] T. Niemelä, H. Niiranen, M. Kellomäki, Self-reinforced composites of bioabsorbable polymer and bioactive glass with different bioactive glass contents. Part II: In vitro degradation, Acta Biomaterialia. 4 (2008) 156–164. doi:10.1016/j.actbio.2007.06.007.

[20] M. Brink, The influence of alkali and alkaline earths on the working range for bioactive glasses, Journal of Biomedical Materials Research. 36 (1997) 109–117. doi:10.1002/(SICI)1097-4636(199707)36:1<109::AID-JBM13>3.0.CO;2-D.

[21] R.F. Brown, M.N. Rahaman, A.B. Dwilewicz, W. Huang, D.E. Day, Y. Li, B.S. Bal, Effect of borate glass composition on its conversion to hydroxyapatite and on the proliferation of MC3T3-E1 cells, Journal of Biomedical Materials Research Part A. 88A (2009) 392–400. doi:10.1002/jbm.a.31679.

[22] M. Ojansivu, A. Mishra, S. Vanhatupa, M. Juntunen, A. Larionova, J. Massera, S. Miettinen, The effect of S53P4-based borosilicate glasses and glass dissolution products on the osteogenic commitment of human adipose stem cells, PLoS ONE. 13 (2018) e0202740. doi:10.1371/journal.pone.0202740.

[23] Q. Fu, M.N. Rahaman, B.S. Bal, L.F. Bonewald, K. Kuroki, R.F. Brown, Silicate, borosilicate, and borate bioactive glass scaffolds with controllable degradation rate for bone tissue engineering applications. II. In vitro and in vivo biological evaluation, Journal of Biomedical Materials Research Part A. 95A (2010) 172–179. doi:10.1002/jbm.a.32823.

[24] L.M. Marquardt, D. Day, S.E. Sakiyama-Elbert, A.B. Harkins, Effects of borate-based bioactive glass on neuron viability and neurite extension: Borate-based Bioactive Glass, J. Biomed. Mater. Res. 102 (2014) 2767–2775. doi:10.1002/jbm.a.34944.

[25] A.L.B. Maçon, T.B. Kim, E.M. Valliant, K. Goetschius, R.K. Brow, D.E. Day, A. Hoppe, A.R. Boccaccini, I.Y. Kim, C. Ohtsuki, T. Kokubo, A. Osaka, M. Vallet-Regí, D. Arcos, L. Fraile, A.J. Salinas, A.V. Teixeira, Y. Vueva, R.M. Almeida, M. Miola, C. Vitale-Brovarone, E. Verné, W. Höland, J.R. Jones, A unified in vitro evaluation for apatite-forming ability of bioactive glasses and their variants, Journal of Materials Science: Materials in Medicine. 26 (2015) 115.

[26] T. Niemela, H. Niiranen, M. Kellomaki, P. Tormala, Self-reinforced composites of bioabsorbable polymer and bioactive glass with different bioactive glass contents. Part I: Initial mechanical properties and bioactivity, Acta Biomaterialia. 1 (2005) 235–242. doi:10.1016/j.actbio.2004.11.002.

[27] T. Kokubo, H. Kushitani, S. Sakka, T. Kitsugi, T. Yamamuro, Solutions able to reproducein vivo surface-structure changes in bioactive glass-ceramic A-W3, Journal of Biomedical Materials Research. 24 (1990) 721–734. doi:10.1002/jbm.820240607.

[28] L. Tirkkonen, H. Halonen, J. Hyttinen, H. Kuokkanen, H. Sievanen, A.-M. Koivisto, B. Mannerstrom, G.K.B. Sandor, R. Suuronen, S. Miettinen, S. Haimi, The effects of vibration loading on adipose stem cell number, viability and differentiation towards bone-forming cells, Journal of The Royal Society Interface. 8 (2011) 1736–1747. doi:10.1098/rsif.2011.0211.

[29] X. Wu, R.E. Youngman, R. Dieckmann, Sodium tracer diffusion and 11B NMR study of glasses of the type (Na2O)0.17(B2O3)x(SiO2)0.83−x, Journal of Non-Crystalline Solids. 378 (2013) 168–176. doi:10.1016/j.jnoncrysol.2013.06.012.

[30] L.-S. Du, J.F. Stebbins, Nature of Silicon−Boron Mixing in Sodium Borosilicate Glasses: A High-Resolution ^{11}B and ^{17}O NMR Study, The Journal of Physical Chemistry B. 107 (2003) 10063–10076. doi:10.1021/jp034048l.

[31]   L.-S. Du, J.F. Stebbins, Solid-state NMR study of metastable immiscibility in alkali borosilicate glasses, Journal of Non-Crystalline Solids. 315 (2003) 239–255. doi:10.1016/S0022-3093(02)01604-6.

[32]   Y. Sun, Z. Zhang, Structural Roles of Boron and Silicon in the CaO-SiO2-B2O3 Glasses Using FTIR, Raman, and NMR Spectroscopy, Metallurgical and Materials Transactions B. 46 (2015) 1549–1554. doi:10.1007/s11663-015-0374-2.

[33]   Y. Lai, Y. Zeng, X. Tang, H. Zhang, J. Han, H. Su, Structural investigation of calcium borosilicate glasses with varying Si/Ca ratios by infrared and Raman spectroscopy, RSC Advances. 6 (2016) 93722–93728. doi:10.1039/C6RA20969F.

[34]   Y. Yu, B. Stevensson, M. Edén, Medium-Range Structural Organization of Phosphorus-Bearing Borosilicate Glasses Revealed by Advanced Solid-State NMR Experiments and MD Simulations: Consequences of B/Si Substitutions, The Journal of Physical Chemistry B. 121 (2017) 9737–9752. doi:10.1021/acs.jpcb.7b06654.

[35]   W. Huang, D.E. Day, K. Kittiratanapiboon, M.N. Rahaman, Kinetics and mechanisms of the conversion of silicate (45S5), borate, and borosilicate glasses to hydroxyapatite in dilute phosphate solutions, Journal of Materials Science: Materials in Medicine. 17 (2006) 583–596. doi:10.1007/s10856-006-9220-z.

[36]   A. Yao, D. Wang, W. Huang, Q. Fu, M.N. Rahaman, D.E. Day, In Vitro Bioactive Characteristics of Borate-Based Glasses with Controllable Degradation Behavior, Journal of the American Ceramic Society. 90 (2007) 303–306. doi:10.1111/j.1551-2916.2006.01358.x.

[37]   X. Liu, W. Huang, H. Fu, A. Yao, D. Wang, H. Pan, W.W. Lu, X. Jiang, X. Zhang, Bioactive borosilicate glass scaffolds: in vitro degradation and bioactivity behaviors, Journal of Materials Science: Materials in Medicine. 20 (2009) 1237–1243. doi:10.1007/s10856-009-3691-7.

[38]   W.C. Lepry, S.N. Nazhat, Highly Bioactive Sol-Gel-Derived Borate Glasses, Chemistry of Materials. 27 (2015) 4821–4831. doi:10.1021/acs.chemmater.5b01697.

[39]   S.J. de Jong, E.R. Arias, D.T.S. Rijkers, C.F. van Nostrum, J.J. Kettenes-van den Bosch, W.E. Hennink, New insights into the hydrolytic degradation of poly(lactic acid): participation of the alcohol terminus, Polymer. 42 (2001) 2795–2802. doi:10.1016/S0032-3861(00)00646-7.

[40]   A.S. Stanislavov, L.F. Sukhodub, L.B. Sukhodub, V.N. Kuznetsov, K.L. Bychkov, M.I. Kravchenko, Structural features of hydroxyapatite and carbonated apatite formed under the influence of ultrasound and microwave radiation and their effect on the bioactivity of the nanomaterials, Ultrasonics Sonochemistry. 42 (2018) 84–96. doi:10.1016/j.ultsonch.2017.11.011.

[41]   C.B. Baddiel, E.E. Berry, Spectra structure correlations in hydroxy and fluorapatite, Spectrochimica Acta. 22 (1966) 1407–1416. doi:10.1016/0371-1951(66)80133-9.

[42]   A. Gand, M. Hindié, D. Chacon, P.R. van Tassel, E. Pauthe, Nanotemplated polyelectrolyte films as porous biomolecular delivery systems: Application to the growth factor BMP-2, Biomatter. 4 (2014) e28823. doi:10.4161/biom.28823.

[43]   S. Eqtesadi, A. Motealleh, A. Pajares, P. Miranda, Effect of milling media on processing and performance of 13-93 bioactive glass scaffolds fabricated by robocasting, Ceramics International. 41 (2015) 1379–1389. doi:10.1016/j.ceramint.2014.09.071.

[44]   M. Ojansivu, A. Mishra, A. Vanhatupa, M. Juntunen, A. Larionova, J. Massera, S. Miettinen, The effect of S53P4-based borosilicate glasses and glass dissolution products on the osteogenic commitment of human adipose stem cells, PlosOne. (2018).

[45]   M. Saito, T. Karakida, R. Yamamoto, T. Nagano, Y. Yamakoshi, T. Hayakawa, S. Oida, K. Gomi, Differentiation potential of osteoblast from cultured C2C12 cells on zirconia disk, Dental Materials Journal. 33 (2014) 275–283. doi:10.4012/dmj.2013-321.

Supplementary data

Figure S1 presents the TGA thermogram of the samples of investigation. As expected, PLA starts decomposing at ~300°C. The decomposition of the PLA ends at ~388°C with a residual mass of ~0.7%. With further heating the mass continues to decrease to reach ~0% at ~670°C. PLA/BAG composites follow the same pattern with PLA decomposition at ~284 and ~280°C for the PLA/13-93B20 and PLA/13-93 respectively. The slight shift toward lower temperature of the PLA thermal degradation in the composite can be assigned to the lower Mw as seen in Table 2. The large mass drop, seen upon heating, ends at ~352°C. The final residual mass is reached and varies with temperature and across samples between 31 and 40%. The average residual mass and standard deviation were measured to be 38±2% and 35±2%, for the PLA/13-93 and PLA/13-93B20, respectively.
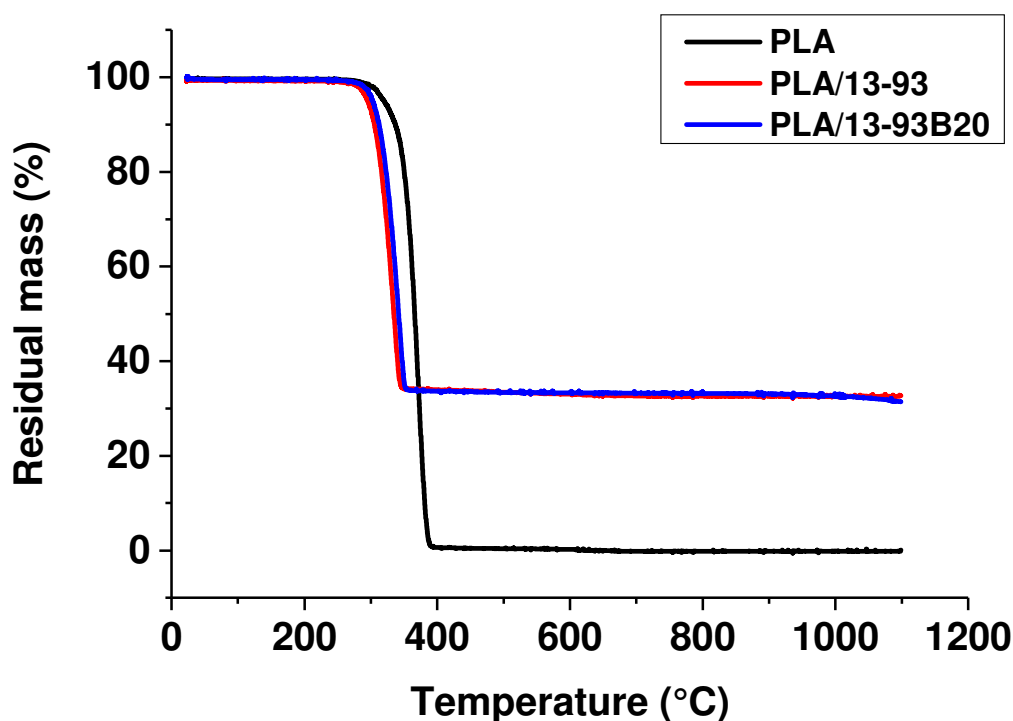

Figure S1: TGA thermogram of the PLA, PLA/13-93 and PLA/13-93B20 obtained at 10°C/min, under N_2 flow, up to 1100°C